Behavioral/Systems/Cognitive

Topographic Distribution, Frequency, and Intensity Dependence of Stimulus-Specific Adaptation in the Inferior Colliculus of the Rat

Daniel Duque,[1] David Pérez-González,[1] Yaneri A. Ayala,[1] Alan R. Palmer,[3] and Manuel S. Malmierca[1,2]

[1]Auditory Neurophysiology Unit, Laboratory for the Neurobiology of Hearing, Institute of Neuroscience of Castilla y León, 37007 Salamanca, Spain [2]Department of Cell Biology and Pathology, Faculty of Medicine, University of Salamanca, 37007 Salamanca, Spain, and [3]Institute of Hearing Research, Medical Research Council, Nottingham NG7 2RD, United Kingdom

The ability to detect unexpected sounds within the environment is an important function of the auditory system, as a rapid response may be required for the organism to survive. Previous studies found a decreased response to repetitive stimuli (standard), but an increased response to rare or less frequent sounds (deviant) in individual neurons in the inferior colliculus (IC) and at higher levels. This phenomenon, known as stimulus-specific adaptation (SSA) has been suggested to underpin change detection. Currently, it is not known how SSA varies within a single neuron receptive field, i.e., it is unclear whether SSA is a unique property of the neuron or a feature that is frequency and/or intensity dependent. In the present experiments, we used the common SSA index (CSI) to quantify and compare the degree of SSA under different stimulation conditions in the IC of the rat. We calculated the CSI at different intensities and frequencies for each individual IC neuron to map the neuronal CSI within the receptive field. Our data show that high SSA is biased toward the high-frequency and low-intensity regions of the receptive field. We also find that SSA is better represented in the earliest portions of the response, and there is a positive correlation between the width of the frequency response area of the neuron and the maximum level of SSA. The present data suggest that SSA in the IC is not mediated by the intrinsic membrane properties of the neurons and instead might be related to an excitatory and/or inhibitory input segregation.

Introduction

The ability to detect unexpected stimuli within the environment is an important function of the brain in general, and of the auditory system in particular, where it mostly depends on some forms of neuronal adaptation (Ulanovsky et al., 2003; Jääskeläinen et al., 2007). The adaptation to repeated sounds while maintaining responsiveness to uncommon ones is known as stimulus-specific adaptation (SSA), and it is thought to be one of the mechanisms that allows novelty detection (Ulanovsky et al., 2003, 2004). SSA was initially described in the auditory cortex (Ulanovsky et al., 2003), but more recently it was found also in the auditory midbrain [inferior colliculus (IC) (Malmierca et al., 2009)] and the thalamus [medial geniculate body (MGB) (Anderson et al., 2009; Yu et al., 2009; Antunes et al., 2010)].

Received July 4, 2012; revised Sept. 18, 2012; accepted Oct. 13, 2012.

Author contributions: A.R.P. and M.S.M. designed research; D.D. performed research; D.D., D.P.-G., and Y.A.A. analyzed data; D.D., D.P.-G., A.R.P., and M.S.M. wrote the paper.

This work was supported by the Spanish Ministerio de Economía y Competitividad (MEC) (BFU2009-07286), Spanish MEC (EUI2009-04083) in the frame of the ERA-NET NEURON (Network of European Funding for Neuroscience Research), to M.S.M. D.D. held a fellowship from the Spanish MEC (BES-2010-035649). D.P.G. held a postdoctoral fellowship from the Botín Foundation. The funders had no role in study design, data collection and analysis, decision to publish, or preparation of this manuscript. The experiments were performed in the Laboratory for the Neurobiology of Hearing, Institute of Neuroscience of Castilla y León, University of Salamanca, Salamanca, Spain. We thank Dr. Nelken and Dr. Caspary for fruitful discussion in a previous version.

Correspondence should be addressed to Manuel S. Malmierca, Institute of Neuroscience of Castilla y León, University of Salamanca, Calle del Pintor Fernando Gallego, 1, 37007 Salamanca, Spain. E-mail: msm@usal.es.

DOI:10.1523/JNEUROSCI.3190-12.2012

 0270-6474/12/3217762-13$15.00/0

The basic properties of SSA have been studied in detail in the auditory cortex (Ulanovsky et al., 2003, 2004; von der Behrens et al., 2009; Taaseh et al., 2011), MGB (Yu et al., 2009; Antunes et al., 2010; Antunes and Malmierca, 2011), and IC (Pérez-González et al., 2005; Malmierca et al., 2009; Lumani and Zhang, 2010; Zhao et al., 2011), but little is known about how it changes within the neuronal receptive field. This is an important issue, since the variation of SSA across the receptive field may shed light on how the neuron's inputs contribute to its generation (Ulanovsky et al., 2004), while a homogeneous SSA would suggest a larger contribution of the intrinsic properties to its origin (Abolafia et al., 2011), although SSA by definition, as opposed to nonspecific adaptation, already suggests that these properties are not involved.

The IC is a key midbrain nucleus that integrates information from all ascending and descending auditory pathways (Malmierca, 2003), and the lowest auditory station where SSA has been found so far. Neurons in the IC project to the auditory cortex via the MGB. Moreover, the IC is the auditory nucleus where the lemniscal and nonlemniscal pathways emerge (for review, see Malmierca, 2003; Lee and Sherman, 2011). This division is relevant because the lemniscal pathway (associated with the central nucleus of the IC) is linked to the processing of basic acoustic features, while the nonlemniscal (lateral, rostral, and dorsal cortices of the IC) (Malmierca et al., 2011) is related to the analysis of more complex features of sound (Hu et al., 1994; Hu, 2003) and multisensory integration (Aitkin et al., 1981; Malmierca et al., 2002). Previous studies on SSA have demonstrated the prevalence of strong SSA in neurons from the nonlem-

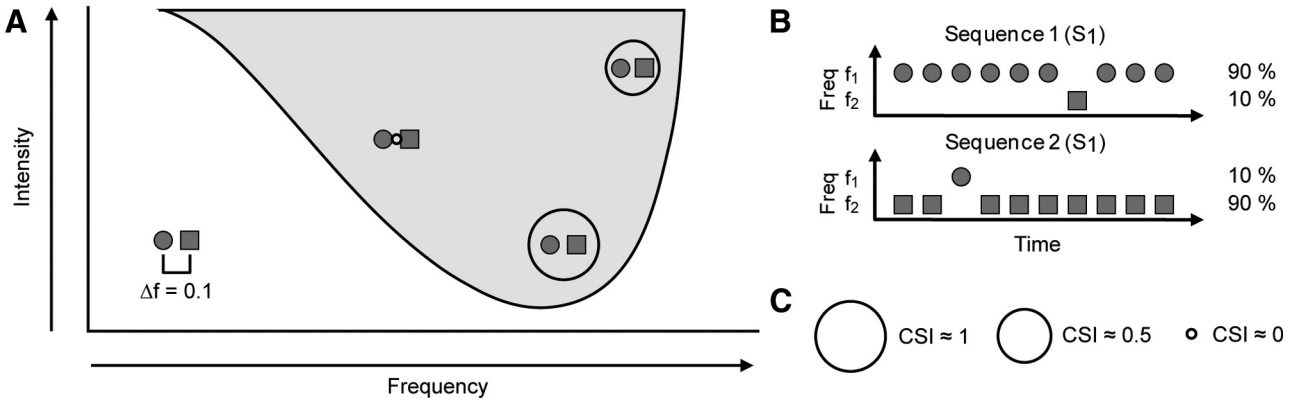

Figure 1. Oddball paradigm and stimulation protocol. ***A***, Schematic FRA showing the protocol of the experiments. Different pairs of frequencies (f_1, circle; f_2, square) were selected within the FRA for the oddball paradigm, covering all the range of frequencies and intensities. The frequency contrast (Δf) between the two frequencies remained constant at 0.1 (0.141 octaves). ***B***, Oddball paradigm. Sequences of 400 pure tones at the two different frequencies were presented, varying the probability of each of the frequencies. In Sequence 1, the f_1 (circle) had 90% probability of occurring, and f_2 (square) had 10%. In Sequence 2, the probabilities of f_1 and f_2 were reversed. After performing the oddball paradigm a CSI value summarizes the SSA seen at that region of the FRA. ***C***, Schematic representation of the CSI value. On top of each pair of frequencies in the FRA, we draw a circle proportional to the CSI: the bigger the circle is, the higher the SSA.

niscal divisions of the IC and MGB (Malmierca et al., 2009; Antunes et al., 2010; Lumani and Zhang, 2010).

In the present account, we quantified and compared the degree of SSA in single neurons of the rat IC, at multiple intensities and frequency combinations, to map the variations of SSA throughout the neuronal receptive field. Moreover, we investigated whether neurons exhibiting a particular response type are better able to encode for SSA and if the spectral properties of the neuronal response affected the level of SSA. Our results demonstrate that SSA is more strongly expressed in the high-frequency region of the receptive field, at low firing rates, and in ON responders. Preliminary reports have been presented previously (Duque et al., 2010, 2011).

Materials and Methods

Surgical procedures. Experiments were performed on 33 adult, female rats (*Rattus norvergicus*, Long Evans) with body weights between 150 and 260 g. All experimental procedures were performed at the University of Salamanca with the approval of, and using methods conforming to the standards of, the University of Salamanca Animal Care Committee. Anesthesia was induced (1.5 g/kg, i.p., 20% solution) and maintained (0.5 g/kg, i.p., given as needed) with urethane. Urethane was chosen as an anesthetic because its effects on multiple aspects of neural activity, including inhibition and spontaneous firing, are known to be less than those of barbiturates and other anesthetic drugs (Hara and Harris, 2002). The respiration was maintained artificially (SAR-830/P Ventilator), monitoring the end-tidal CO_2 level (CapStar-100). For this purpose, the trachea was cannulated and atropine sulfate (0.05 mg/kg, s.c.) was administered to reduce bronchial secretions. Details of surgical procedures have been described previously (Pérez-González et al., 2005; Malmierca et al., 2009; Antunes et al., 2010). Body temperature was maintained at 38 ± 1°C by means of a heating blanket. The animal was placed in a stereotaxic frame in which the ear bars were replaced by hollow speculae that accommodated a sound delivery system, inside a sound-sealed room.

Acoustic stimuli and electrophysiological recording. A craniotomy was performed to expose the cerebral cortex overlying the IC. Extracellular single-unit responses were recorded using a tungsten electrode (1–2 MΩ) (Merrill and Ainsworth, 1972) lowered through the cortex by means of a piezoelectric microdrive (Burleigh 6000 ULN). Neuron location in the IC was based on stereotaxic coordinates, physiological criteria of tonotopicity and response properties (Malmierca et al., 2003; Hernández et al., 2005; Pérez-González et al., 2005, 2006; Malmierca et al., 2009), and confirmed histologically afterward.

Acoustic stimuli were delivered through a sealed acoustic system (Malmierca et al., 2009) using two electrostatic loudspeakers (TDT EC1; Tucker Davis Technologies) driven by two TDT ED1 modules. The stimuli were presented contralaterally to the recording side; search stimuli were pure tones or noise bursts monaurally delivered under computer control using TDT System II hardware and custom software (Faure et al., 2003; Pérez-González et al., 2005, 2006; Malmierca et al., 2008). The output of the system at each ear was calibrated *in situ* using a ¼ inch condenser microphone (model 4136; Brüel and Kjær) and a DI-2200 spectrum analyzer (Diagnostic Instruments). The maximum output of the TDT system was flat from 0.5 to 4 kHz (~110 ± 7 dB SPL), from 4.5 to 14.5 kHz (~90 ± 6 dB SPL), and from 15.5 to 40 kHz (~95 ± 7 dB SPL), presenting a notch at 15 kHz. The highest frequency produced by this system was limited to 40 kHz. The second and third harmonic components in the signal were ≤40 dB below the level of the fundamental at the highest output level (Malmierca et al., 2008, 2009).

Action potentials were recorded with a BIOAMP amplifier (Tucker Davis Technologies), the 10× output of which was further amplified and bandpass filtered (TDT PC1; f_c, 500 Hz and 3 kHz) before passing through a spike discriminator (TDT SD1). Spike times were logged with a resolution of ≈150 μs on a computer by feeding the output of the spike discriminator into an event timer (TDT ET1) synchronized to a timing generator (TDT TG6). Stimulus generation and on-line data visualization were controlled with custom software. Spike times were displayed as dot rasters sorted by the acoustic parameter varied during testing.

From an isolated neuron, the approximate frequency tuning was audiovisually determined by presenting pure tones lasting 75 ms with a 5 ms rise/fall time (Hernández et al., 2005). We obtained the frequency response area (FRA), the combination of frequencies and intensities capable of evoking a response, as an estimation of the neuronal receptive field. For that, we presented multiple combinations of frequency and intensity using an automated procedure with 5–10 stimulus repetitions at each frequency (from 0.5 to 40 kHz, in 20–30 logarithmic steps, presented randomly) and intensity (10 dB steps, presented from lower to higher intensities). The spike counts evoked at each combination of frequency and intensity were then plotted using MATLAB. We used this representation of the FRA to calculate the minimum threshold and best frequency (BF) of response, i.e., the frequency where the minimum threshold is found.

Stimulus presentation paradigms. The representation of the FRA allowed us to choose pairs of frequencies (f_1 and f_2) within the response area of the neuron that elicited a similar firing rate at the same intensity level (Fig. 1*A*). Both frequencies in each pair were always presented at the same sound level. For each pair of frequencies, stimuli were presented in an oddball paradigm similar to that used to record mismatch negativity responses in human (Näätänen, 1992) and animal (Ulanovsky et al., 2003, 2004; Malmierca et al., 2009; Antunes et al., 2010) studies. Briefly, a train of 400 stimuli containing both frequencies f_1 and f_2 was presented

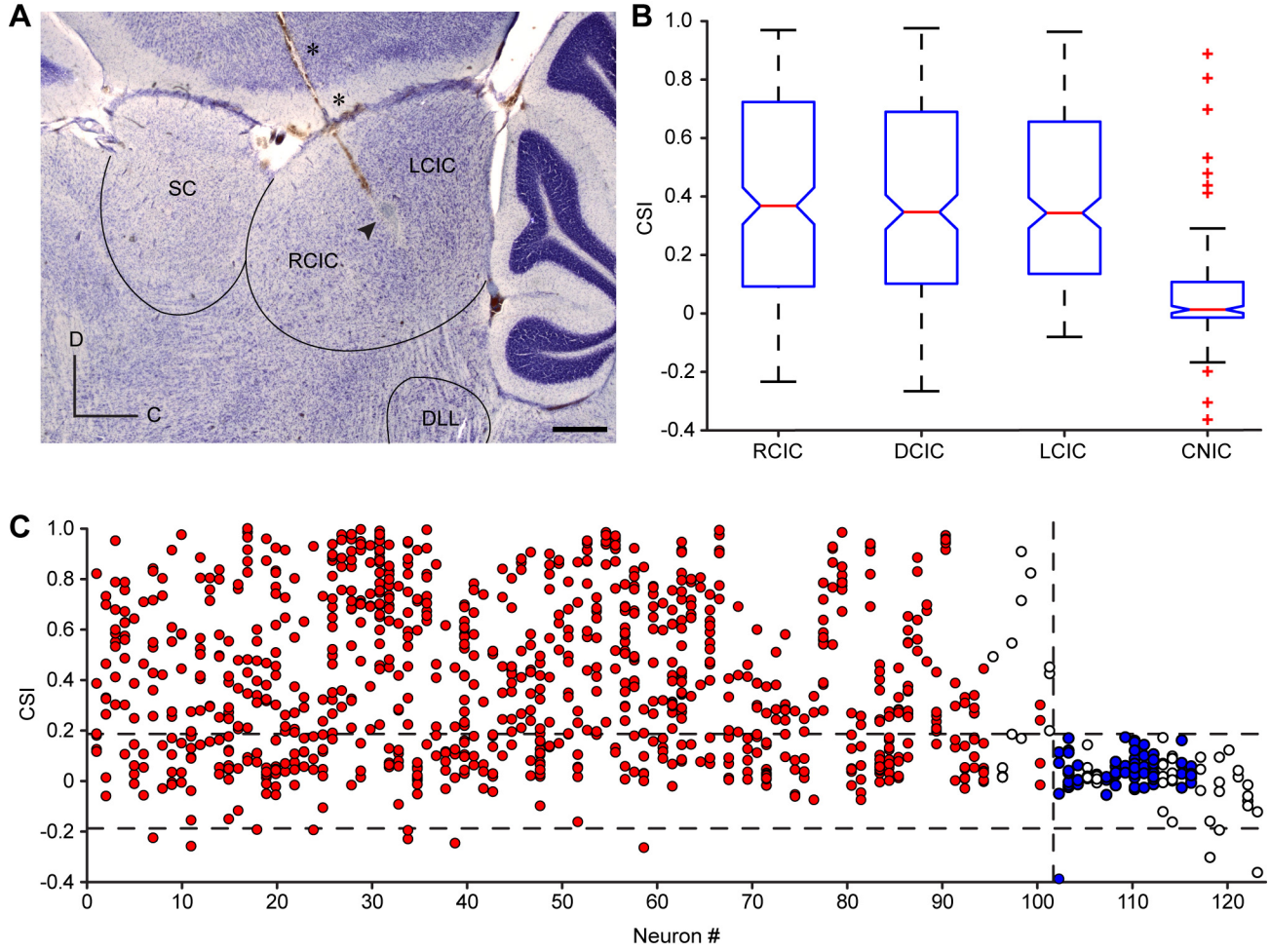

Figure 2. Anatomical location of CSI. ***A***, Photomicrography showing a sagittal section of the IC with a typical electrode track (asterisks) and the electrolytic lesion generated (arrowhead). Scale bar, 500 μm. C, Caudal; D, dorsal. ***B***, Box plot with the median value (red line) of CSI sorted by anatomic regions. The blue box delimits the 25th and 75th percentiles, and dashed lines show the most extreme data points not considered outliers. Red crosses indicate outliers. Cortical regions (RCIC, DCIC, and LCIC) are significantly different from the CNIC (Kruskal–Wallis test, $p < 0.001$). ***C***, Neuronal CSI variability. Each dot illustrates the level of CSI for a given pair of frequencies. Any single neuron can present levels of CSI close to 1 and below 0, depending on the region of the FRA. Red dots are values from neurons that present adapting pairs of frequencies, blue dots are values from neurons that only have nonspecifically adapting pairs of frequencies, and empty dots are pairs of frequencies in identified CNIC neurons. The top dashed line shows the higher cutoff value (0.18), the bottom one shows the lower cutoff value (−0.18), and the vertical dash line illustrates the separation between adapting and nonspecifically adapting neurons. SC, Superior colliculus; DLL, dorsal lateral lemniscus.

under the oddball paradigm: one frequency (f_1) was presented as the standard (90% occurrence), while, interspersed randomly among the standards, the deviant stimuli (10% occurrence) were presented at the second frequency (f_2). After obtaining one data set, the relative probabilities of the two stimuli were reversed, with f_2 as the standard and f_1 as the deviant (Fig. 1*B*). Dot raster plots (see Fig. 3) are used to illustrate the responses obtained to the oddball paradigm, plotting individual spikes (red dots indicate responses to the deviant; blue dots indicate responses to the standard). Stimulus presentations are marked along the vertical axis. The responses to the standard and deviant stimuli were expressed as spikes per stimulus, to account for the different number of presentations in each condition, due to the different probabilities. The frequency contrast remained constant under all the experimental conditions at $\Delta f = 0.10$, where $\Delta f = (f_2 - f_1)/(f_2 \times f_1)^{1/2}$. (Ulanovsky et al., 2003, 2004; Malmierca et al., 2009). This value is equivalent to a frequency separation of 0.141 octaves. The stimuli were presented at a repetition rate of 4 Hz. These conditions have been shown previously to evoke strong SSA in the IC (Malmierca et al., 2009).

The degree of SSA was quantified by calculating the common SSA index (CSI) from the responses (firing rate) elicited in the oddball condition. The CSI has been used in previous studies (Ulanovsky et al., 2003, 2004; Malmierca et al., 2009; Antunes et al., 2010) and is defined as $CSI = [d(f_1) + d(f_2) - s(f_1) - s(f_2)]/[d(f_1) + d(f_2) + s(f_1) + s(f_2)]$, where $d(f)$ and $s(f)$ are responses to each frequency f_1 or f_2 when they were the deviant (d) or standard (s) stimulus, respectively. This index reflects the extent to which the response to the standard was suppressed or the response to the deviant was enhanced (Fig. 1*C*). The possible range of CSI values is from −1 to +1, being positive if the response to the deviant stimulus is greater. To avoid including the spontaneous activity in the analysis, we set time windows chosen individually in each case. We had a default time window that embraced the whole stimulus (10 to 85 ms) for low spontaneous activity responses (see Fig. 3*B*,*C*) and, in those cases where the spontaneous rate was higher (see Fig. 3*A*,*D*), it was possible to set the boundaries based on the shape of the peristimulus time histogram (PSTH). When probing for SSA at different frequencies and intensities, we started to collect the data from the lowest intensity at BF and then gradually chose different pairs of frequencies covering (1) frequencies lower and higher than the BF and (2) all the possible range of intensity levels, in 10 dB steps. There is no a priori octave spacing when choosing the pairs, but we always try to test at both the low- and the high-frequency edges of the FRA, choosing two stimuli that evoked similar firing rates to ensure that all differences in response were due to the statistics of the stimulus ensemble.

Histological verification and recording sites. Each track was marked with electrolytic lesions (10–15 μA for 10–15 s) for subsequent histological localization of the neurons recorded (Fig. 2*A*). At the end of each exper-

iment, the animal was given a lethal dose of sodium pentobarbital and perfused transcardially with PBS (0.5% $NaNO_3$ in PBS) followed by fixative (a mixture of 1% paraformaldehyde and 1% glutaraldehyde in rat Ringer's solution). The brain tissue was sectioned in the sagittal plane into 40-μm-thick sections that were Nissl stained with 0.1% cresyl violet. Recording sites were marked on standard sections from a rat brain atlas (Paxinos and Watson, 2005), and units were assigned to one of the four main divisions of the IC (Malmierca et al., 1993, 1995, 2011; Loftus et al., 2008): lateral cortex (LC), rostral cortex (RC), dorsal cortex (DC), or central nucleus (CN). This information was complemented and confirmed by the stereotaxic coordinates used during the experiment to localize the IC.

Results

To study how SSA varies within the receptive field of IC neurons, we recorded the responses from 124 well-isolated single units throughout the IC while presenting stimuli in an oddball paradigm. For all neurons, we determined the FRA and used the oddball paradigm choosing several pairs of frequencies at different intensities within the FRA (Fig. 1*A*). We used a constant frequency contrast ($\Delta f = 0.1$), repetition rate (4 Hz), and probability of occurrence of the deviant stimuli (10%).

SSA is better encoded in the nonlemniscal pathway

We localized histologically 81 of the 124 recorded neurons (65.3%) to the different IC subdivisions (Fig. 2). Twenty-five of them were from the rostral cortex (RCIC, 31%), 21 from the lateral cortex (LCIC, 26%), and 17 from the dorsal cortex (DCIC, 21%). Eighteen were localized to the central nucleus (CNIC, 22%). The Kruskal–Wallis one-way ANOVA by ranks shows that the distributions of CSI values obtained in the cortical regions were similar among them (median ± interquartile range, DCIC, 0.367 ± 0.629; RCIC, 0.346 ± 0.587; LCIC, 0.343 ± 0.520), but significantly different from those of the CNIC (0.012 ± 0.116; $p = 1.35 \cdot 10^{-13}$; Dunn's method confirmed differences between each cortical region and the CNIC, $p < 0.05$ in all cases; Fig. 2*B*). Although the level of SSA in the CNIC is distinctly low, seven pairs of frequencies from neurons histologically located in the edges of the CNIC exhibited significant SSA (CSI, >0.4; Fig. 2*B*). Since our sample is consistent and biased to the cortical regions of the IC (almost the 80% of the neurons were localized in cortical regions), in the subsequent analysis we have included all the recorded neurons instead of only the 81 localized histologically, and we will no longer consider regional subdivisions.

SSA varies within the FRA

From the 124 recorded neurons, we obtained a total of 1057 different pairs of frequencies. On average, we tested nine pairs of frequencies per neuron (range, 3–24 pairs per neuron). Pairs of frequencies that did not respond to both stimuli in the oddball paradigm ($n = 68$) were excluded from the analysis. Figure 2*C* shows the individual variability of the CSI value for all the neurons in our sample. Since our main goal was a detailed analysis of neurons that exhibit SSA, we established a cutoff to prevent the neurons lacking SSA (as those located in the CNIC) from masking or averaging out the relationship between SSA sensitivity and other response properties under study. We used a CSI value of +0.18 as threshold for significant SSA, since the intrinsic variability of the response could evoke positive values of CSI that are not related to a specifically stronger response to the deviant stimulus. This cutoff value was established previously by Antunes et al. (2010) by choosing the most negative CSI value in the data set (−0.18) to represent the most extreme variance due to random fluctuations in spike counts. We calculated the cutoff value for the present data set obtaining a value of −0.21, but we considered that the different cutoff values obtained are due to the experimental variability rather than a genuine difference. Thus, for consistency we use the same value as used previously. We consider the range of CSI between −0.18 and +0.18 as an indication of a lack of stimulus-specific adaptation. Thus, a CSI value above 0.18 indicates significant SSA. The few values in our data set below −0.18 (11 of 1057, 1%) are considered outliers. Neurons that presented all their CSI values below 0.18 are referred to as "nonspecifically adapting" neurons. One-hundred and two neurons (82.3%; 900 pairs of frequencies) showed high SSA levels (CSI, >0.18) for at least one of the pairs of frequencies analyzed. The remaining 22 neurons (17.7%) showed a low SSA (CSI, ≤0.18) for all pairs of frequencies analyzed (89 pairs of frequencies). Interestingly, 12 of the 18 neurons that we localized in the CNIC presented such low SSA (Fig. 2*C*, empty dots).

Figure 3 shows four examples of individual neurons with their corresponding FRA. For each neuron, we display dot raster plots obtained using the oddball paradigm with a pair of frequencies that show strong adaptation (left columns) and with a pair that do not show adaptation (right columns). The corresponding PSTHs are also shown. To assess the variability of SSA within the FRA, we plotted the pairs of frequencies tested (represented by dots in the FRA) and the level of SSA of each pair of frequencies (represented by a circle, with the diameter proportional to the CSI value; Fig. 1*C*). Figure 3*A* shows a broadly V-shaped FRA where 13 pairs of frequencies were tested. Figure 3*B* shows a multipeaked FRA (18 pairs of frequencies), while Figure 3*C* shows a narrow FRA (9 pairs of frequencies), and Figure 3*D* a mosaic FRA (8 pairs of frequencies). In all these cases, the PSTHs exhibit a larger response to the deviant sounds (red line), showing that the neuron presents SSA to some pairs of frequencies (left columns) and a similar response for both conditions when it is not differentially adapted (right columns).

To see how CSI values are distributed throughout the whole auditory receptive field of the rat, we first merged the firing rates of all the FRAs to create a cumulative receptive field (Fig. 4*A–D*). This cumulative FRA was created over the whole range of frequencies (from 0.5 to 40 kHz) and intensities (between −20 and 80 dB SPL) that we tested. The resulting cumulative receptive field obtained was a broadly tuned, V-shaped-like FRA that presented the lowest threshold (−20 dB SPL) at ~12 kHz. Then, we plotted the center frequency [$CF = (f_2 \times f_1)^{1/2}$] of each pair of frequencies on top of the cumulative receptive field, grouped according to the level of SSA that they elicited, as shown in Fig. 4. For convenience, we established four different groups: CSI < 0.18 ($n = 284$; Fig. 4*A*), 0.18 < CSI < 0.5 ($n = 277$; Fig. 4*B*), 0.5 < CSI < 0.75 ($n = 183$; Fig. 4*C*), and CSI > 0.75 ($n = 156$; Fig. 4*D*). The distribution of the frequencies analyzed with low CSI values (CSI < 0.18; Fig. 4*A*) was spread throughout the entire FRA, covering the whole range of frequencies and intensities used, but a majority of pairs of frequencies tended to be located at the high-intensity regions of ~10–12 kHz, which are also the highest firing rate regions (yellow and red areas). In contrast, the highest CSI values (>0.75; Fig. 4*D*) were concentrated in the lower firing rate areas (dark blue), which are located at low and medium intensities around the 10–12 kHz region, and also at high frequencies. It is important to note that there were no pairs with CSI values >0.75 found in the low-frequency tail of the "synthetic" receptive field. Medium CSI values (0.18 < CSI < 0.75; Fig. 4*B*,*C*) show an intermediate localization. In this case the distribution of the pairs was not as homogeneous as the one

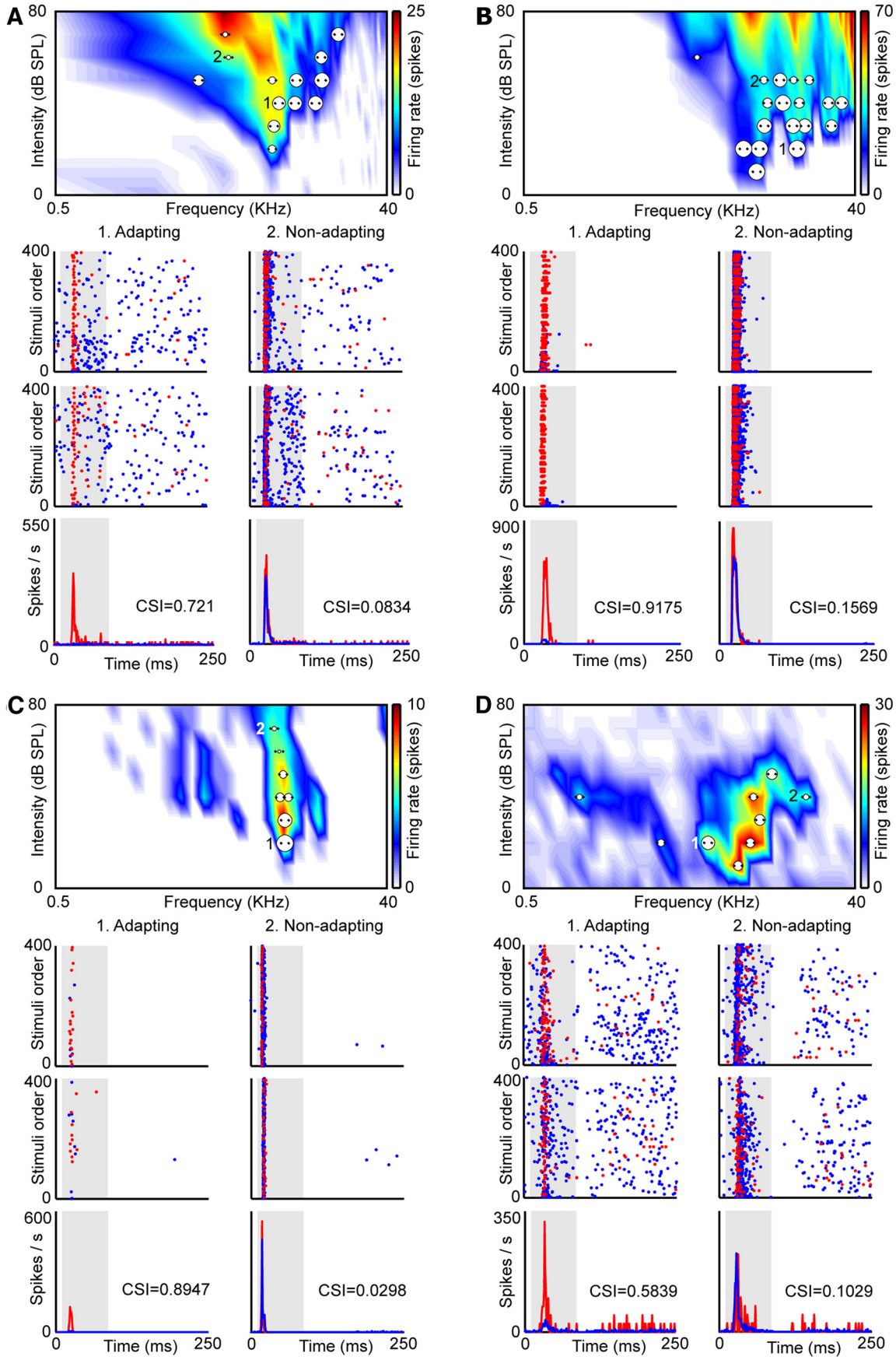

Figure 3. Examples of neurons. ***A–D***, Each panel shows the FRA (broad V-shaped FRA, ***A***; multipeaked FRA, ***B***; narrow FRA, ***C***; mosaic FRA, ***D***) of a neuron and all the pairs of frequencies analyzed as dots. Each pair of dots is associated to a circle the size of which is proportional to the level of CSI evoked. Examples of an adapting pair of frequencies are marked as 1, (*Figure legend continues*.)

observed with low CSI levels, but instead began to show a trend toward low firing rates.

To further analyze the parameters that could affect the strength of SSA, we divided our data into different groups according to the two main sound parameters (i.e., intensity and frequency). First, we created different groups taking into account sound level (decibels of SPL; Fig. 4*E*): the results showed an emerging trend such that SSA is higher at low sound intensities. Next, we analyzed how the SSA of the IC neurons varied as a function of the sound frequency that we used for stimulation (from 0.5 to 40 kHz). For this purpose, we calculated the center frequency for each pair of frequencies and arranged them in 0.5-octave-wide groups. As shown in Figure 4*F*, high CSI values are clearly skewed toward high frequencies. We finally merged all the information relative to CSI and plotted it together, taking into account the intensity (in decibels of SPL) and the frequency of each pair of frequencies analyzed (in kilohertz) to understand how SSA varies as a function of these two parameters (Fig. 4*G*). High and low SSA levels are differently distributed. Neurons exhibit the highest CSI values in the regions with frequencies above 10 kHz at low intensities and also at relative high intensities at high frequencies (Fig. 4*G*, yellow–red). In contrast, the lowest values of CSI (Fig. 4*G*, green–blue) are confined to high intensities and to low frequencies.

At this juncture, to better visualize where the SSA is strongest within the FRA, we replotted the graph in Figure 4*G*, but this time considering the distances relative to the threshold (reTh) and the best frequency of each neuron. In Figure 5*A*, we clearly observe that the highest CSI values are concentrated at the high-frequency edge. To check that we do not have any bias due to high-frequency neurons, we standardized the data to the high-frequency edge (Fig. 5*B*). This analysis confirms that the results are genuine and not due to a data sampling bias. This plot reinforces the idea that larger CSI values are found at high frequencies and low intensities within the FRA of individual neurons, demonstrating that SSA is not a property homogeneously distributed within the FRA of the neuron.

With the aim of quantifying these effects, we performed a three-way ANOVA, where the three factors evaluated were the frequency, the intensity, and the effect of the neuron (as a random factor). The results of this analysis showed that intensity ($F = 112.75$; $p = 7.18 \cdot 10^{-44}$), frequency ($F = 52.25$; $p = 4.69 \cdot 10^{-22}$), and neuron ($F = 9.33$; $p = 4.01 \cdot 10^{-79}$) are major factors that shape the level of CSI.

SSA as a function of sound intensity

To understand how SSA varies through the intensity range, we established six different groups in 10 dB steps above each neuron's minimum threshold, and we calculated the median CSI value in each group separately (Fig. 6*A*). The maximum intensity that we played was +70 dB reTh. Thus, we pooled together the +60 and the +70 dB reTh groups to make the high-intensity group more reliable. CSI values close to the threshold are significantly larger than those at higher intensity levels (Kruskal–Wallis test, $p < 0.001$). *Post hoc* comparisons confirmed that all groups were significantly different to those at least 20 dB apart (Dunn's method, $p < 0.05$; Fig. 6*A*).

In an attempt to understand the correlation between the intensity level and the firing rate, we performed an additional analysis where we considered that the effect of the intensity might be due to firing rate dependence. For this reason, we took the frequency pairs above 70 dB SPL and sorted them in three groups according to the firing rate observed in the region of the FRA where we choose the pairs: low (<1.5 spikes/stimulation), middle (1.5 to 4 spikes/stimulation), and high (>4 spikes/stimulation) firing rates. A Kruskal–Wallis test showed that there are no significant differences between the groups (low firing rate, 0.200; middle firing rate, 0.141; high firing rate, 0.098; $p = 0.516$). Thus, lower CSI levels at high intensities are independent of the firing rate.

To analyze the relationship between sound level and the latency of the neuronal response, we plotted the latency differences between the standard and the deviant stimuli (defined as the difference between the median first spike latency to the standard and the deviant condition for each frequency) as a function of the different intensity groups that we previously established (Fig. 6*B*). The results demonstrate that there were no significant differences between the intensity groups (Kruskal–Wallis test, $p = 0.172$; Table 1).

To study the time course of adaptation in the IC population, we examined how responses changed over the 400 consecutive trials. Figure 6*C* shows the average population response as a function of trial number for both standard (blue trace) and deviant stimuli (red trace). In the three groups of intensities analyzed (low intensities, ≤20 dB reTh, Fig. 6*C*, left; medium intensities, 30–40 dB reTh, middle; high intensities, ≥50 dB reTh, right), a reduction of the response to the standard stimulus occurred rapidly (blue trace), reaching a minimum within the first 50–100 trials, while the response to the oddball stimulus (red trace) showed little adaptation over the course of the train of stimuli. A power law equation ($y = a * x^b + c$) provided the best fit to the responses to the standard across trials for all conditions. A high proportion of the adaptation to the standard stimulus was explained by this model (low intensities, $r^2 = 0.923$; medium intensities, $r^2 = 0.952$; high intensities, $r^2 = 0.955$; $p < 0.0001$ for all conditions). In contrast, the responses to the deviant stimuli fit poorly to this regression model ($r^2 < 0.1$ in all conditions). A close inspection of the dynamics of adaptation reveals that intensity level affects inversely the rate of adaptation to the standard stimuli, determined by b ($b_{low} = -0.627$; $b_{med} = -0.657$; $b_{high} = -0.577$), i.e., at higher intensities the adaptation is slower [95% confidence interval (CI_{95}) at high intensities, −0.5982 to −0.5569; CI_{95} at medium intensities, −0.6791 to −0.6346; CI_{95} at low intensities, −0.6554 to −0.5993]. This suggests that at high sound levels this reduction of the firing rate is not enough to allow an adequate discrimination between the standard and the deviant stimuli (Fig. 6*C*, right), a result that reflects the lower level of adaptation seen at these intensities. It is important to know that the firing rate does not saturate at high intensities (the firing rate keeps increasing gradually from 50 to 80 dB reTh in a monotonic way) (data not shown), so it is unlikely that the firing rate is putting a ceiling on SSA.

←

(*Figure legend continued.*) and examples of a nonspecifically adapting pair of frequencies are marked as 2. Below the FRA we show the dot raster plots obtained in the adapting pair (left) and in the nonspecifically adapting pair (right). The blue dots represent spikes evoked by the standard stimulus (90% probability), while the red dots represent those evoked by the deviant stimulus (10% probability). Stimulus presentations are accumulated in the temporal domain in the vertical axis. In the adapting examples, red dots are more visible because of the specific decrease of the response to the standard stimulus. The top panels are the ones obtained after using Sequence 1 in the oddball paradigm; middle panels are the ones obtained after Sequence 2 under the oddball paradigm. Bottom panels are the PSTHs, averaged for both frequencies when deviant (red) or standard (blue). CSI values obtained in each pair of frequencies are showed as insets in the PSTHs. The shaded backgrounds in the dot raster and PSTH plots indicate the duration of the stimulus.

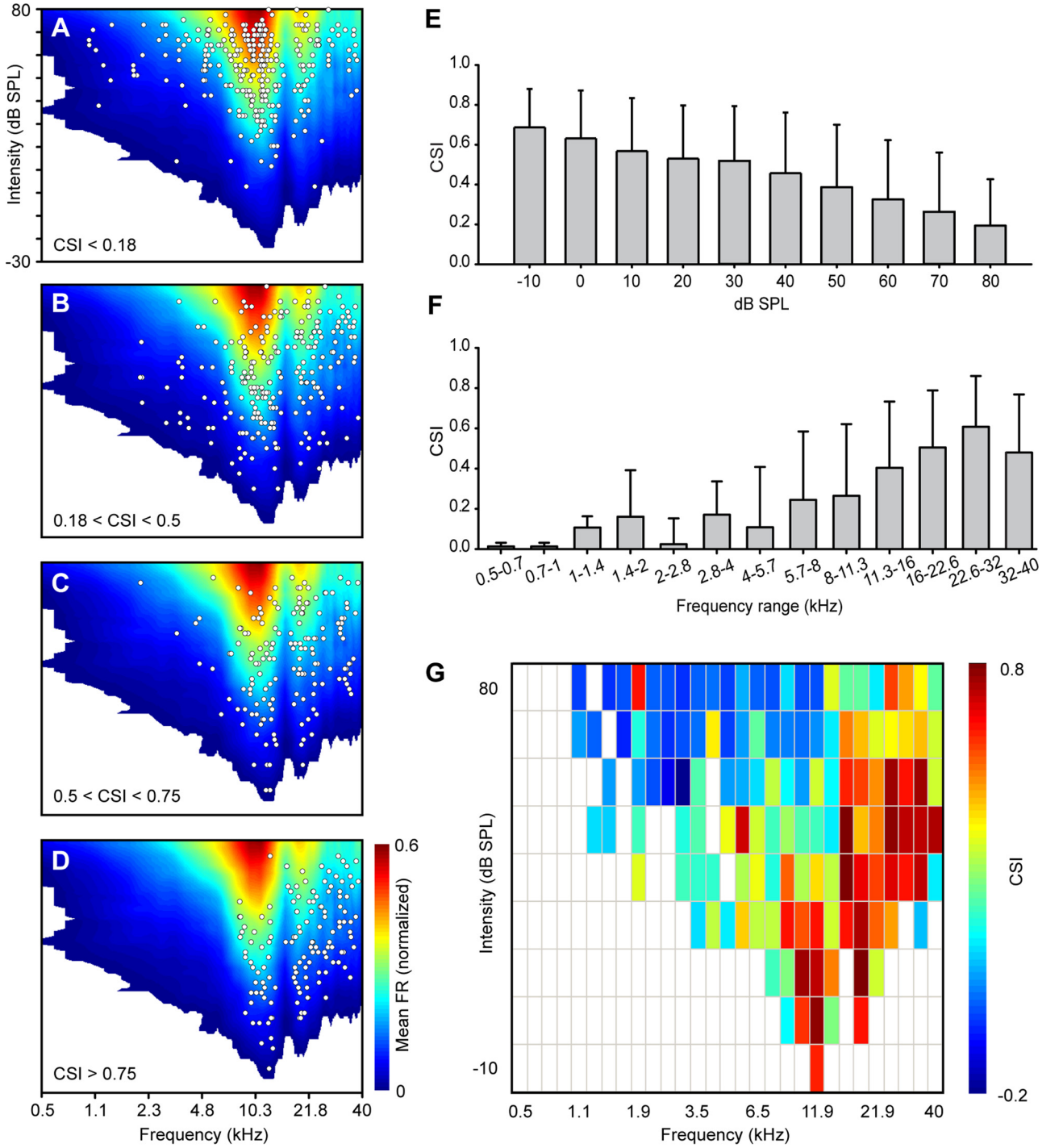

Figure 4. Localization of the frequency pairs in the auditory receptive field sorted by CSI. ***A–D***, Cumulative FRA generated by averaging all the FRAs in our sample. The response was normalized to the maximum firing rate of each individual neuron before pooling the FRAs. Each white dot represents the center of a pair of frequencies tested. ***A***, Topographic location within the FRA where the lowest CSI levels (<0.18) were found. ***B***, ***C***, Topographic location for middle levels of CSI (0.18 to 0.5, ***B***; 0.5 to 0.75, ***C***). ***D***, Topographic location of the pairs of frequencies that evoked the highest CSI levels (>0.75). ***E***, Distribution of the levels of CSI sorted by absolute intensities (decibels of SPL). ***F***, Distribution of the levels of CSI sorted by absolute frequencies (0.5 octaves steps, in kilohertz). ***G***, Raw distribution of the CSI values considering absolute intensity (decibels of SPL, 10 dB steps) and frequency (in kilohertz, grouped in 0.5 octave steps). Note the different distribution of high CSI values (warm colors) and low CSI values (cold colors). Error bars indicate SD.

SSA as a function of sound frequency

Next, to check whether the trend of high SSA toward high frequencies is related to the absolute sound frequency (i.e., neurons tuned to high frequencies show stronger SSA) or whether it is actually integrated across the receptive field of the neurons, we established five different groups based on the distance to the best frequency of each neuron: very low frequencies (more than −1 octave of distance from the BF), low frequencies (between −1 and −0.2 octaves of distance from BF), medium frequencies (±0.2 octaves of distance from BF), high frequencies (between 0.2 and 1 octaves of distance from BF), and very high frequencies (>1 octave of distance from the BF). The 0.4 octave window around the BF was set to integrate similar, but not strictly equal pairs of frequencies. The 2 octave window was set to differentiate

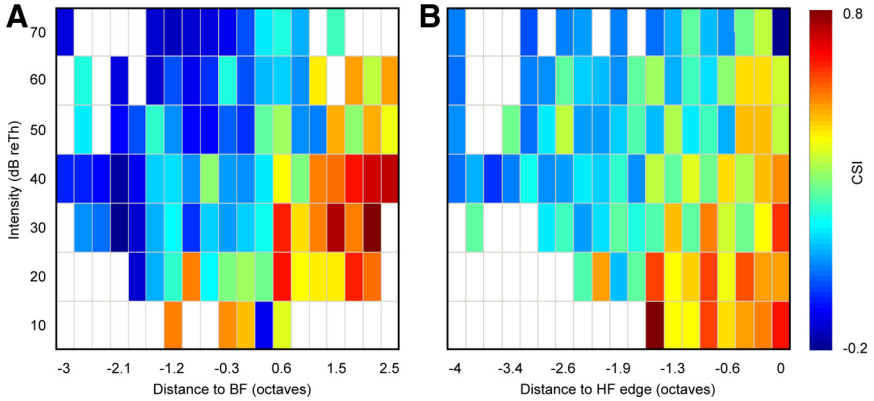

Figure 5. Summary of the distribution of the levels of CSI in the FRA. Mean CSI values found in the neurons as a function of intensity and frequency. ***A***, Distribution of the CSI values sorted relatively to the BF and the threshold of the FRA. High CSI values are concentrated at the high-frequency edge. ***B***, Distribution of the CSI values relative to the high-frequency (HF) edge of the FRA for each frequency pair. The values are also standardized to the threshold of each FRA. The distribution of high CSI values along a vertical line demonstrates that there is not a bias due to high-frequency neurons.

the most distant parts of the FRA. Figure 7*A* shows that CSI values in the high-frequency region are significantly larger than those values in the low-frequency one (Kruskal–Wallis test, $p < 0.001$). *Post hoc* comparisons confirmed differences between groups (Dunn's method, $p < 0.05$ in all comparisons but those between low and very low, and high and very high frequencies, which were not significant).

Then, we plotted the latency difference based on the five groups established previously. Figure 7*B* shows that the latency difference tends to be larger for frequencies above BF (Kruskal–Wallis test, $p < 0.001$). Dunn's *post hoc* analysis confirmed differences between groups (Fig. 7*B*). In that case, the latency of both standard and deviant is shorter at the best frequency (Table 2) and then increases when the frequencies are more distant to the best frequency. Latencies are slightly larger at the high-frequency region compared to the ones at the low frequency region.

Last, we analyzed the time course of adaptation, establishing three groups relative to the BF of each neuron: low frequencies (less than −0.2 octaves from BF), best frequency (between −0.2 and 0.2 octaves), and high frequencies (>0.2 octaves from BF; Fig. 7*C*). As for the intensity analysis described above, a power law equation was the best fit of the response to the standard tone: low frequencies, $r^2 = 0.933$; best frequency, $r^2 = 0.952$; and high frequencies, $r^2 = 0.951$ ($p < 0.0001$ for all conditions). Deviant stimuli responses fit poorly to this regression model ($r^2 < 0.1$ in all conditions). These results show that the frequency relative to the BF affects the dynamics of adaptation by allowing a greater discrimination between the standard and the deviant sounds at high frequencies than at low frequencies. Although the speed of adaptation to the standard stimulus is higher around the BF ($b_{low} = -0.592$; $b_{BF} = -0.659$, $b_{high} = -0.595$; CI_{95} around BF, −0.6814 to −0.6370; CI_{95} at low frequencies, −0.6178 to −0.5666; CI_{95} at high frequencies, −0.6167 to −0.5734), the decrement of the response to the standard stimulus is larger at high frequencies than at the lower ones, exhibiting a larger amount of adaptation at this frequency range.

SSA in relation to the temporal pattern of the neuronal response

An important feature of the neuronal responses is their temporal pattern. Thus, we also studied whether the type of response could be related to the level of SSA. We classified the neuronal responses of our sample in five different groups: ON, LONG-LATENCY ON, ON-SUSTAINED, SUSTAINED, and ON-OFF (Rees et al., 1997) (Fig. 8). ON responses showed a robust response confined to the first 40 ms of the stimulus. The LONG-LATENCY ON response started 50–80 ms after the beginning of the tone. ON-SUSTAINED responses exhibited a clear ON response followed by a SUSTAINED portion, with a lower firing rate than the ON portion. We defined the ON part of the ON-SUSTAINED response as the early portion with a higher firing rate (at least 50% more than the sustained portion). SUSTAINED responses showed a constant response that lasts 50 ms or more. To further analyze whether there were differences on SSA between the ON and the SUSTAINED portion of the SUSTAINED response, we defined the ON portion as the first 20 ms of response. The ON-OFF response had two different latency components in the response, with an ON and OFF portion (after the ending of the stimulus). In our sample, we did not find any pauser or regular-chopper responses, which are typical of the CNIC (Rees et al., 1997).

As reported previously (Hind et al., 1963; Rees et al., 1997), IC neurons can exhibit different patterns of response depending on the region under examination within the FRA. However, at this point, we should emphasize that the majority of the neurons in our sample are from outside the CNIC (Fig. 2). In some cases analyzing the responses of a pair of frequencies, each frequency can present a different pattern of response (i.e., one frequency evokes an ON response and the other one an ON-SUSTAINED response), and also the same frequency can respond differently when the sound is frequent or rare. Thirty-four pairs of frequencies were not analyzed for this reason. Our sample includes 679 pairs of frequencies that showed an ON response, 123 that were ON-SUSTAINED, 16 that were SUSTAINED, 21 that were ON-OFF, and 27 that were LONG-LATENCY ON. Sometimes (21 of 87 neurons, 24.14%) increasing the sound level caused the response of a neuron to change from an ON response to a SUSTAINED (2 of 87), ON-OFF (4 of 87), or ON-SUSTAINED response (15 of 87).

As expected from previous work (Pérez-González et al., 2005; Malmierca et al., 2009), the analysis of the strength of SSA as a function of the response type (Fig. 8*A*) shows that the ON responses evoke the larger CSI. The median SSA in ON types (CSI, 0.401) was significantly different from that in ON-SUSTAINED (CSI, 0.235) and SUSTAINED (CSI, 0.059) types (Kruskal–Wallis ANOVA on ranks, $p < 0.001$; *post hoc* Dunn's method analysis confirmed differences with $p < 0.05$). The same analysis also showed differences between the ON type and the OFF portion of the ON-OFF response (CSI, 0.153; p values the same for Kruskall–Wallis and Dunn's). Additionally, CSI values of the ON portion in the ON-OFF response are larger than the values of the OFF portion: these data suggest that the ON portion of the whole neuronal response is more sensitive to SSA.

To further analyze this effect, we examined whether the ON portion of the ON-SUSTAINED, SUSTAINED, and ON-OFF responses better encoded the SSA (Fig. 8*B*). In the ON-SUSTAINED and the ON-OFF responses, we observed a signifi-

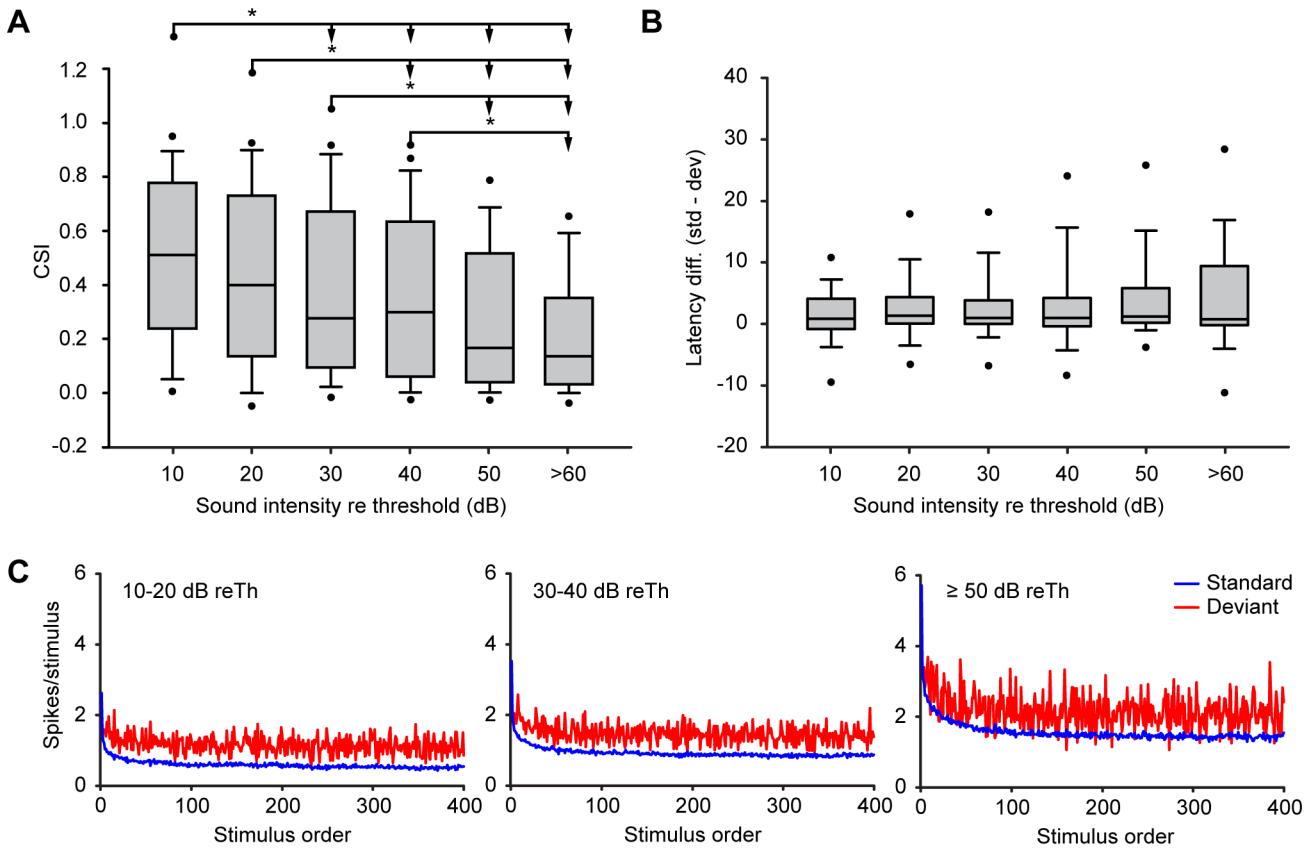

Figure 6. CSI analysis by intensity. ***A***, Box plots showing the distribution of the levels of CSI sorted by intensities relative to the neuronal threshold. The asterisks indicate significant differences (Kruskal–Wallis test, $p < 0.001$; Dunn's method, $p < 0.05$). ***B***, Box plots of the latency difference (in milliseconds) between deviants and standards, sorted by intensities relatives to threshold. In both charts (***A*** and ***B***), the middle line represents the median value, the box delimits the 25th and 75th percentiles, whiskers indicate the 10th and 90th percentiles, and the dots indicate the 5th and 95th percentiles. ***C***, Time course of adaptation sorted by intensities relative to the neuronal threshold. Blue lines show the time course of the standard tones, and red lines show the time course of the deviant tones. Left, Mean time course of the response at low intensities (10–20 dB reTh). Middle, Middle intensities (30–40 dB reTh). Right, High intensities (≥50 dB reTh).

Table 1. Median values of the latency of the response (in milliseconds) per intensity

Intensity (dB reTh)	Median first spike latency (ms)		Latency difference (ms)
	Standard	Deviant	
10	23.84	21.30	0.58
20	20.86	18.82	1.09
30	18.78	17.62	0.70
40	19.49	18.72	0.69
50	17.60	16.62	0.95
<60	18.63	18.18	0.53

cant difference in the CSI levels between the ON portion and the SUSTAINED/OFF portion (Wilcoxon signed rank test, $Z = -5.053$, $p > 0.001$; Mann–Whitney rank sum test, $t = 344$, $p = 0.028$, respectively), whereas in the SUSTAINED response there were no significant differences between the levels founds in the ON and the SUSTAINED portions (Wilcoxon signed rank test, $Z = -1.099$, $p = 0.296$). As before, these data indicate that a distinct ON portion of the response better encodes SSA.

To evaluate the relationship between the type of response and the latency of the response, we considered the latency difference (Fig. 8*C*): we observed that the latency difference was significantly larger in the ON-SUSTAINED responses than in the ON and the LONG-LATENCY ON responses (Kruskal–Wallis ANOVA on ranks, $p < 0.001$; *post hoc* Dunn's method analysis, $p < 0.05$ in the two cases). This distinction was correlated with a more prominent effect of inhibition over the ON than the SUSTAINED region of the response (Pérez-González et al., 2012), causing the standard response to be reduced or abolished in the ON and LONG-LATENCY ON cases (short latency difference), but being unable to do the same in the ON-SUSTAINED case (longer latency difference).

SSA in relation to spectral properties of the neuronal response

Last, we studied how the type of FRA is related to the level of SSA. For this purpose we classified the FRAs into six different groups: multipeaked/U-shaped ($n = 48$), V-shaped ($n = 20$), mosaic ($n = 12$), narrow ($n = 9$), closed ($n = 3$), and low tilt ($n = 3$) (Le Beau et al., 2001; Hernández et al., 2005). There were no high-tilt FRAs in our sample. For convenience, multipeaked and U-shaped FRAs were pooled into a single broadly tuned group. Since our data are biased to the cortical regions of the IC, a majority of the neurons are multipeaked (Hernández et al., 2005). To avoid a bias due to low CSI values at high intensities, we computed only the highest CSI value obtained in each neuron. The data demonstrate that the level of SSA for all the neurons was independent of the FRA type and is similar in all the FRAs analyzed (data not shown; Kruskal–Wallis ANOVA on ranks, $p = 0.185$).

To further analyze the variation of the SSA with the shape of the response area, we evaluated the bandwidth of each FRA related to (1) the region of the IC (Fig. 9*A*) and (2) the level of SSA

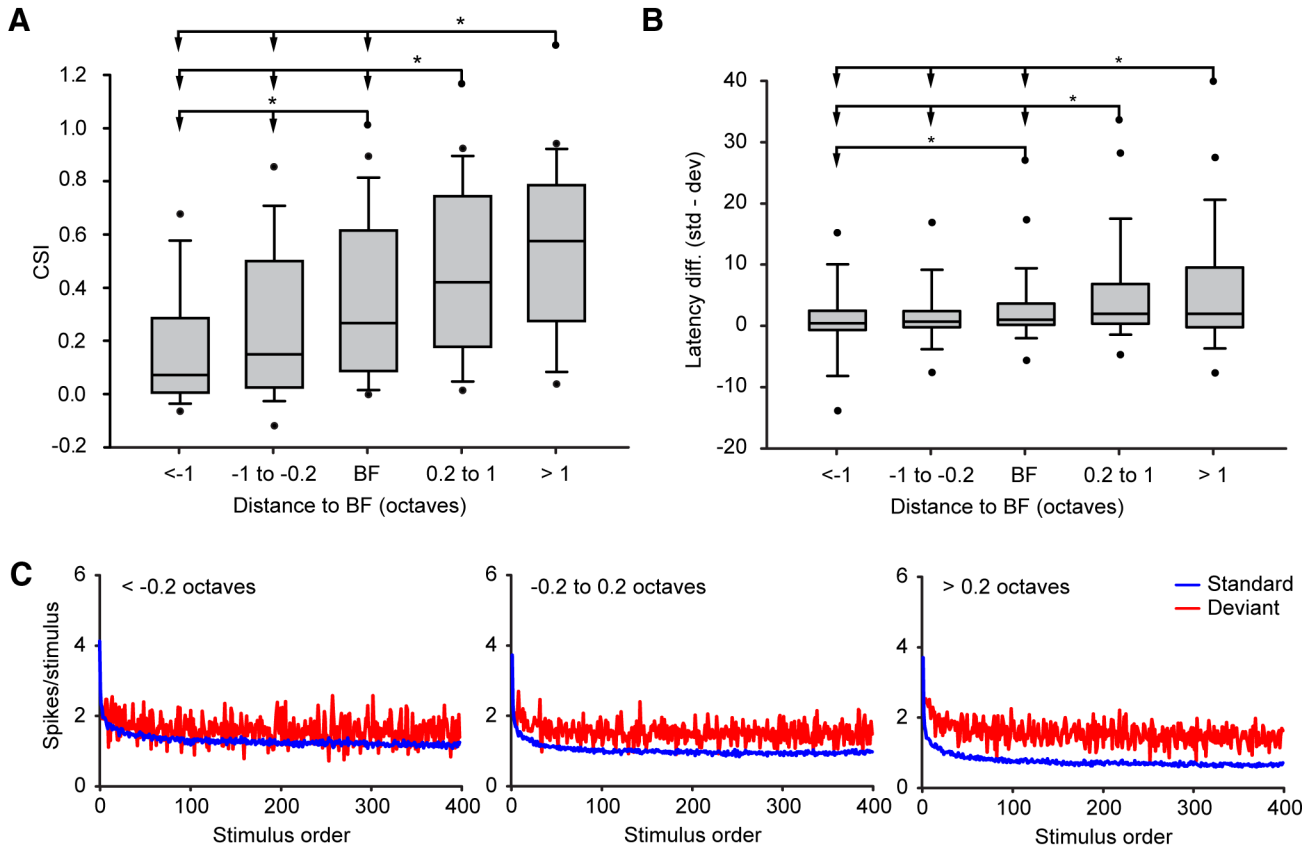

Figure 7. CSI analysis by frequency. ***A***, Box plots showing the distribution of the levels of CSI sorted by frequencies relative to the neuronal best frequency (in octaves). The asterisks indicate significant differences (Kruskal–Wallis test, $p < 0.001$; Dunn's method, $p < 0.05$). ***B***, Box plots of the latency difference (in milliseconds) sorted by frequencies relative to the neuronal BF. The asterisks indicate significant differences with the Kruskal–Wallis test ($p < 0.001$) and Dunn's method ($p < 0.05$). In both charts (***A*** and ***B***), the middle line represents the median value, the box delimits the 25th and 75th percentiles, whiskers indicate the 10th and 90th percentiles, and the dots indicate the 5th and 95th percentiles. ***C***, Time course of adaptation sorted by frequencies relative to the neuronal BF. Blue lines show the time course of the standard tones, and red lines show the time course of the deviant tones. Left, Mean time course of the response at low frequencies (−0.2 octaves lower). Middle, Middle frequencies (−0.2 to 0.2 octaves). Right, High frequencies (≥0.2 octaves).

Table 2. Median values of the latency of the response (in milliseconds) per frequency

Distance to BF (octaves)	Median first spike latency (ms)		Latency difference (ms)
	Standard	Deviant	
Less than −1	19.82	18.79	0.09
−1 to −0.2	18.66	18.72	0.33
−0.2 to 0.2	17.96	17.23	0.68
0.2 to 1	22.22	19.49	1.58
>1	23.01	19.69	1.57

(*B*). The CSI groups we used were the same as we had used before (Fig. 4). Despite the clear trend, we did not find significant differences between the groups in the region analysis either at 10 or 40 dB reTh (Kruskal–Wallis ANOVA on ranks, 10 dB reTh, $p = 0.633$; 40 dB reTh, $p = 0.073$). In the CSI groups we did not find significant differences at 10 dB reTh (Kruskal–Wallis ANOVA on ranks, $p = 0.117$), but we found differences at 40 dB reTh ($p < 0.024$; *post hoc* Dunn's method confirmed differences between CSIs <0.18 and >0.75). To make the analysis more robust, we pooled the cortical regions (LCIC, RCIC, and DCIC) into a single group, and we did the same with the three adapting groups (0.18 to 0.5, 0.5 to 0.75, and >0.75). *T* tests confirmed that cortical regions had broader FRA (*t* test, 40 dB reTh, $t = 351$; $p = 0.014$) and that the broader the FRA is, the higher the CSI levels are (*t* test, 40 dB reTh, $t = 669$; $p = 0.005$).

Discussion

Our results demonstrate that in the IC, SSA is not constant within the neuronal receptive field, and therefore is not a characteristic property of the neuron. In most cases, a single neuron can exhibit CSI values as high as 1 in some regions of the FRA as well as values close to 0 in others. Our study further demonstrates that higher levels of SSA are biased toward low intensity levels and to the high-frequency edge of the FRA. Furthermore, the type of temporal response pattern observed in each particular region of the FRA is also related to the magnitude of the CSI. Thus, the ON responses exhibit larger SSA values than other response types. We also demonstrated that the neurons with broader receptive fields show more SSA, and most of them are located in the cortical regions of the IC.

Comparison with previous studies and technical considerations

Previous studies of SSA based on the oddball paradigm considered only a single pair of frequencies or a very restricted area of the neurons' receptive field (Bauerle et al., 2011). In the present study, we show a robust set of data (recording up to 24 pairs of frequencies per neuron) that reveals that SSA sensitivity is not homogeneous, but rather varies across the response area. Thus, a single CSI value cannot be used to completely define the sensitivity for neuronal SSA.

Our study confirms that neurons from the nonlemniscal pathway in IC have higher SSA sensitivity (Malmierca et al., 2009).

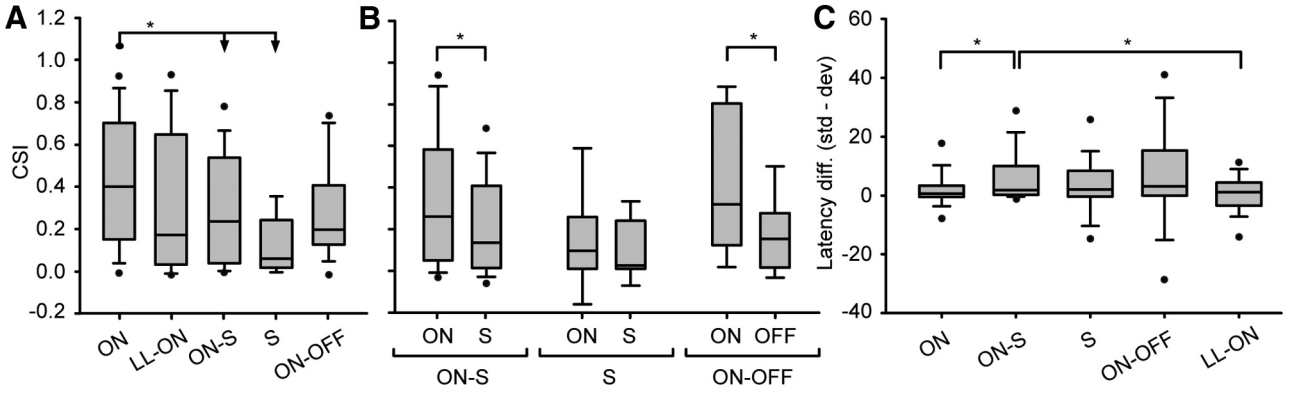

Figure 8. CSI analysis by pattern of response. ***A***, Box plot showing the CSI values distributed by the type of response: ON, LONG-LATENCY ON (LL-ON), ON-SUSTAINED (ON-S), SUSTAINED (S), and ON-OFF. The asterisks indicate significant differences (Kruskal–Wallis test, $p < 0.001$; Dunn's method, $p < 0.05$). ***B***, Comparison of the CSI values evoked in the ON and SUSTAINED regions of the ON-S and S responses, and the ON and OFF regions in the ON-OFF response. The asterisks indicate significant differences (Wilcoxon test, $p < 0.001$ and Mann–Whitney test, $p = 0.028$, respectively). ***C***, Box plots representing the median latency difference (black line) sorted by the type of response. The asterisks indicate significant differences (Kruskal–Wallis test, $p < 0.001$; Dunn's method, $p < 0.05$). In all cases, the middle line represents the median value, the edges of the box delimit the 25th and 75th percentiles, whiskers indicate the 10th and 90th percentiles, and the dots indicate the 5th and 95th percentiles.

Neurons in the LCIC, DCIC, and RCIC have the largest and less oriented dendritic arbors in the IC (Malmierca et al., 1993, 1995, 2011), allowing neurons to integrate inputs over a broader frequency range. As we show here (Fig. 9*A*), neurons in the IC cortex possessed broader FRAs. Although the data do not show correlations between the three factors (CSI, bandwidth, and IC subdivisions), it is likely that the higher levels of SSA found in the cortical regions are related to the width of the FRA. Similar relations between adaptation, anatomical subdivisions, and the shape of the FRA have been shown previously in the external cortex of the barn owl (Gutfreund and Knudsen, 2006), a structure homologous to the same region in the rat IC (Knudsen, 1983; Gutfreund and Knudsen, 2006).

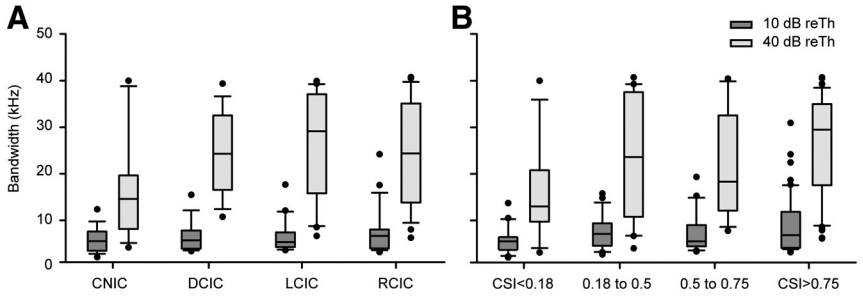

Figure 9. Relationship between bandwidth and CSI. Box plots showing the median value of the bandwidth (in kilohertz) of the FRA at 10 dB above threshold (10 dB reTh; dark gray boxes) and 40 dB over threshold (40 dB reTh; light gray boxes) are shown. ***A***, Median values of the bandwidth as a function of anatomical IC location. ***B***, Median values of bandwidth sorted by the maximum level of CSI evoked in the FRA (0.18 to 0.5, CSI of <0.5; 0.5 to 0.75, CSI of <0.75; >0.75, CSI of <1). In both charts, the middle line represents the median value, the edges of the box delimit the 25th and 75th percentiles, whiskers indicate the 10th and 90th percentiles, and the dots illustrate all outliers.

Our results support previous studies that reported that SSA is stronger for the ON responses of the neurons both in the IC (Pérez-González et al., 2005; Malmierca et al., 2009; Lumani and Zhang, 2010; Zhao et al., 2011) and the MGB (Antunes et al., 2010; Antunes and Malmierca, 2011). Moreover, our data demonstrate that the ON portion of other response types with a well-defined ON region, like ON-OFF and ON-SUSTAINED responses, show larger SSA as well.

A previous study (Bauerle et al., 2011) concluded that higher levels of SSA were associated with the outer regions of the FRA at high intensity levels. This is partially in agreement with our results. However, we found increased levels of SSA only at the high-frequency domain, regardless of the intensity of the stimulus. Since we used a different animal model and anesthesia as well as different analytical tools and studied different auditory regions, it is difficult to make comparisons and reconcile the discrepancies between these studies.

It remains unknown whether or not the frequency and intensity biases that we demonstrate here have behavioral relevance for rats. Because of the time required to obtain data, we focused on stimulation parameters (frequency contrast, $\Delta f = 0.1$; interstimulus interval, 4 Hz) that have been proven previously to elicit consistent and large SSA (Malmierca et al., 2009; Antunes et al., 2010). Further experiments are needed to test whether other conditions that have an effect on SSA (i.e., different frequency separations or repetition rates) would yield comparable results.

SSA is stronger near the neuron's threshold and on the high-frequency side of the response area

The most important finding of this paper is that low sound intensities and high frequencies evoke stronger SSA than other frequency-level combinations. Because of the adaptation process, the response to the standard stimulus at low intensities disappears gradually after a few repetitions, resulting in a high CSI. During this process, the latency of the response to the standard stimulus increases compared to the latency of the responses to the deviant (Table 1). At high intensities, the response to the standard stimulus is more sustained, and the net result is a low CSI value, because there is no shift in the latency to the standard stimulus due to adaptation. It has been shown that both GABA and glycine control the nonmonotonicity (Faingold et al., 1991), the temporal responses (Le Beau et al., 1996), and the FRA shape of many IC neurons (Le Beau et al., 2001). Although similar mechanisms may be involved in producing SSA, it is unlikely that inhibition alone could explain the differences in CSI values within the intensity domain, because inhibition plays a less prominent role in controlling these factors, i.e., nonmonotonicity, at low intensities

(Sivaramakrishnan et al., 2004). Indeed, a previous study performed in our laboratory demonstrated that $GABA_A$ mediated inhibition mainly acts by controlling the gain of the responses, so this type of inhibition plays a minor role in the generation of SSA (Pérez-González et al., 2012). However, since GABA mainly affects the fast component of adaptation (Pérez-González et al., 2012) and the adaptation to the standard is faster at low and middle intensities, it is apparent that multiple mechanisms could be interacting to generate SSA.

Another important feature that we have revealed here is that SSA is significantly stronger on the high-frequency edge of the FRA. Moreover, latency differences at high frequencies show that the latency of the response to the standard tone is larger than that to the deviant stimulus (Fig. 5*C*), implying that there is some specific effect on the standard tone in the high-frequency range of responses that is not present in the low-frequency range. Since inhibition precedes excitation in many IC neurons, (Fubara et al., 1996) and GABA inhibition affects SSA (Pérez-González et al., 2012), it is tempting to speculate that the high values of latency difference at high frequencies might relate to an early inhibitory input that holds back the response to the standard sound (Table 2), which in turn would create the differences in the SSA values between the low- and the high-frequency sounds that we observed.

SSA mechanisms and functional significance

The frequency dependence of SSA may be explained by (1) different inputs to the same neuron, depending mostly on frequency, and the existence of different processes of adaptation associated with these inputs (Ulanovsky et al., 2004); (2) a lateral inhibition network (de la Rocha et al., 2008) based on a broader inhibitory field (Wu et al., 2008); and/or (3) the presence of dual and differential inhibitory effects that will affect SSA differentially, one acting primarily in the low-frequency range, the other at high frequency. In bats, Williams and Fuzessery (2011) showed that there are two non-completely overlapping inhibitory receptive fields that shape FM selectivity. These two inhibitory regions arise from different neurochemical inputs: the low-frequency region is mostly under the influence of GABA, whereas the high-frequency region is under the influence of glycine. Whether or not similar inhibitory mechanisms based on this differential effect of GABA and glycine can account for the frequency/intensity dependence of SSA awaits future studies. Another potential mechanism that could contribute to SSA in the IC is the intrinsic membrane properties of the neuron (Abolafia et al., 2011), but this is unlikely because one would expect individual neurons to show a unique CSI value for each neuron, and here we have demonstrated that SSA depends on the specific frequencies that are tested.

SSA, at least in rat auditory cortex, seems to depend on adaptation with a bandwidth of about one-third of an octave (Taaseh et al., 2011). Since our experiments were performed over a narrow frequency range (0.141 octaves), smaller than the suggested width of the adaptation channels estimated by Taaseh et al. (2011), it could be that such adaptation channels are narrower at low intensities. That would explain the differences between low and high intensities, because narrow channels will allow cross-frequency adaptation at low intensities, but not at high intensities, where the channel will be wider than the frequency separations that we used for this experiment.

SSA lies upstream of the generation of MMN (mismatch negativity) (Ulanovsky et al., 2003; Nelken and Ulanovsky, 2007; Taaseh et al., 2011), a late component of auditory ERP (Näätänen et al., 1978). While a previous study showed that SSA does not depend on NMDA receptors, whereas MMN does (Farley et al., 2010), Taaseh et al. (2011) suggested that, at least in auditory cortex, SSA shows true deviance detection, as does MMN. It is likely that biasing SSA toward the low-intensity domain of the FRA, as well as to the highest spectral continuum, might help to sharpen sound discrimination (hyperacuity), as suggested by Bitterman et al. (2008). Future studies should analyze whether IC neurons are also sensitive to the violation of the regularity of the tone sequence caused by the presentation of the deviant stimuli (Jacobsen and Schroger, 2001, 2003), because there is growing and convincing evidence that the human auditory brainstem is able to encode regularities in the auditory stimulation history that serve to detect novel events (Grimm et al., 2011; Slabu et al., 2010, 2012).

In conclusion, our study demonstrates that SSA is not a characteristic property homogeneously distributed within the neuronal receptive field, and further, it suggests that at the population level, SSA is a major property of most nonlemniscal IC neurons well suited to the notion that subcortical neurons exhibiting SSA may contribute upstream to the generation of MMN.

References

Abolafia JM, Vergara R, Arnold MM, Reig R, Sanchez-Vives MV (2011) Cortical auditory adaptation in the awake rat and the role of potassium currents. Cereb Cortex 21:977–990. CrossRef Medline

Aitkin LM, Kenyon CE, Philpott P (1981) The representation of the auditory and somatosensory systems in the external nucleus of the cat inferior colliculus. J Comp Neurol 196:25–40. CrossRef Medline

Anderson LA, Christianson GB, Linden JF (2009) Stimulus-specific adaptation occurs in the auditory thalamus. J Neurosci 29:7359–7363. CrossRef Medline

Antunes FM, Malmierca MS (2011) Effect of auditory cortex deactivation on stimulus-specific adaptation in the medial geniculate body. J Neurosci 31:17306–17316. CrossRef Medline

Antunes FM, Nelken I, Covey E, Malmierca MS (2010) Stimulus-specific adaptation in the auditory thalamus of the anesthetized rat. PLoS One 5:e14071. CrossRef Medline

Bäuerle P, von der Behrens W, Kössl M, Gaese BH (2011) Stimulus-specific adaptation in the gerbil primary auditory thalamus is the result of a fast frequency-specific habituation and is regulated by the corticofugal system. J Neurosci 31:9708–9722. CrossRef Medline

Bitterman Y, Mukamel R, Malach R, Fried I, Nelken I (2008) Ultra-fine frequency tuning revealed in single neurons of human auditory cortex. Nature 451:197–201. CrossRef Medline

de la Rocha J, Marchetti C, Schiff M, Reyes AD (2008) Linking the response properties of cells in auditory cortex with network architecture: cotuning versus lateral inhibition. J Neurosci 28:9151–9163. CrossRef

Duque D, Malmierca MS, Pérez-González D (2010) Frequency and intensity dependent properties of stimulus-specific adaptation in the inferior colliculus. Paper presented at Ninth International Conference of Neuroethology, Salamanca, Spain, August.

Duque D, Pérez-González D, Malmierca MS (2011) Stimulus-specific adaptation in the inferior colliculus: effects of frequency, intensity and firing rate. Paper presented at Thrity-fourth Research Meeting of the Association for Research in Otolaryngology, Baltimore, MD, February.

Faingold CL, Boersma Anderson CA, Caspary DM (1991) Involvement of GABA in acoustically-evoked inhibition in inferior colliculus neurons. Hear Res 52:201–216. CrossRef Medline

Farley BJ, Quirk MC, Doherty JJ, Christian EP (2010) Stimulus-specific adaptation in auditory cortex is an NMDA-independent process distinct from the sensory novelty encoded by the mismatch negativity. J Neurosci 30:16475–16484. CrossRef Medline

Faure PA, Fremouw T, Casseday JH, Covey E (2003) Temporal masking reveals properties of sound-evoked inhibition in duration-tuned neurons of the inferior colliculus. J Neurosci 23:3052–3065. Medline

Fubara BM, Casseday JH, Covey E, Schwartz-Bloom RD (1996) Distribution of GABAA, GABAB, and glycine receptors in the central auditory

system of the big brown bat, *Eptesicus fuscus*. J Comp Neurol 369:83–92. CrossRef Medline

Grimm S, Escera C, Slabu L, Costa-Faidella J (2011) Electrophysiological evidence for the hierarchical organization of auditory change detection in the human brain. Psychophysiology 48:377–384. CrossRef Medline

Gutfreund Y, Knudsen EI (2006) Adaptation in the auditory space map of the barn owl. J Neurophysiol 96:813–825. CrossRef Medline

Hara K, Harris RA (2002) The anesthetic mechanism of urethane: the effects on neurotransmitter-gated ion channels. Anesth Analg 94:313–318, table of contents. CrossRef Medline

Hernández O, Espinosa N, Pérez-González D, Malmierca MS (2005) The inferior colliculus of the rat: a quantitative analysis of monaural frequency response areas. Neuroscience 132:203–217. CrossRef Medline

Hind JE, Goldberg JM, Greenwood DD, Rose JE (1963) Some discharge characteristics of single neurons in the inferior colliculus of the cat. II. Timing of the discharges and observations on binaural stimulation. J Neurophysiol 26:321–341. Medline

Hu B (2003) Functional organization of lemniscal and nonlemniscal auditory thalamus. Exp Brain Res 153:543–549. CrossRef Medline

Hu B, Senatorov V, Mooney D (1994) Lemniscal and non-lemniscal synaptic transmission in rat auditory thalamus. J Physiol 479:217–231. Medline

Jääskeläinen IP, Ahveninen J, Belliveau JW, Raij T, Sams M (2007) Short-term plasticity in auditory cognition. Trends Neurosci 30:653–661. CrossRef Medline

Jacobsen T, Schroger E (2001) Is there pre-attentive memory-based comparison of pitch? Psychophysiology 38:723–727. CrossRef Medline

Jacobsen T, Schroger E (2003) Measuring duration mismatch negativity. Clin Neurophysiol 114:1133–1143. CrossRef Medline

Knudsen EI (1983) Subdivisions of the inferior colliculus in the barn owl (*Tyto alba*). J Comp Neurol 218:174–186. CrossRef Medline

Le Beau FE, Rees A, Malmierca MS (1996) Contribution of GABA- and glycine-mediated inhibition to the monaural temporal response properties of neurons in the inferior colliculus. J Neurophysiol 75:902–919. Medline

LeBeau FE, Malmierca MS, Rees A (2001) Iontophoresis in vivo demonstrates a key role for GABA(A) and glycinergic inhibition in shaping frequency response areas in the inferior colliculus of guinea pig. J Neurosci 21:7303–7312. Medline

Lee CC, Sherman SM (2011) On the classification of pathways in the auditory midbrain, thalamus, and cortex. Hear Res 276:79–87. CrossRef Medline

Loftus WC, Malmierca MS, Bishop DC, Oliver DL (2008) The cytoarchitecture of the inferior colliculus revisited: a common organization of the lateral cortex in rat and cat. Neuroscience 154:196–205. CrossRef Medline

Lumani A, Zhang H (2010) Responses of neurons in the rat's dorsal cortex of the inferior colliculus to monaural tone bursts. Brain Res 1351:115–129. CrossRef Medline

Malmierca MS (2003) The structure and physiology of the rat auditory system: an overview. Int Rev Neurobiol 56:147–211. CrossRef Medline

Malmierca MS, Blackstad TW, Osen KK, Karagülle T, Molowny RL (1993) The central nucleus of the inferior colliculus in rat: a Golgi and computer reconstruction study of neuronal and laminar structure. J Comp Neurol 333:1–27. CrossRef Medline

Malmierca MS, Seip KL, Osen KK (1995) Morphological classification and identification of neurons in the inferior colliculus: a multivariate analysis. Anat Embryol (Berl) 191:343–350. CrossRef Medline

Malmierca MS, Merchán MA, Henkel CK, Oliver DL (2002) Direct projections from cochlear nuclear complex to auditory thalamus in the rat. J Neurosci 22:10891–10897. Medline

Malmierca MS, Hernández O, Falconi A, Lopez-Poveda EA, Merchán M, Rees A (2003) The commissure of the inferior colliculus shapes frequency response areas in rat: an *in vivo* study using reversible blockade with microinjection of kynurenic acid. Exp Brain Res 153:522–529. CrossRef Medline

Malmierca MS, Izquierdo MA, Cristaudo S, Hernández O, Pérez-González D, Covey E, Oliver DL (2008) A discontinuous tonotopic organization in the inferior colliculus of the rat. J Neurosci 28:4767–4776. CrossRef Medline

Malmierca MS, Cristaudo S, Pérez-González D, Covey E (2009) Stimulus-specific adaptation in the inferior colliculus of the anesthetized rat. J Neurosci 29:5483–5493. CrossRef Medline

Malmierca MS, Blackstad TW, Osen KK (2011) Computer-assisted 3-D reconstructions of Golgi-impregnated neurons in the cortical regions of the inferior colliculus of rat. Hear Res 274:13–26. CrossRef Medline

Merrill EG, Ainsworth A (1972) Glass-coated platinum-plated tungsten microelectrodes. Med Biol Eng 10:662–672. CrossRef Medline

Näätänen R (1992) Attention and brain function. Hillsdale, NJ: Erlbaum.

Näätänen R, Gaillard AW, Mantysalo S (1978) Early selective-attention effect on evoked potential reinterpreted. Acta Psychol (Amst) 42:313–329. CrossRef Medline

Nelken I, Ulanovsky N (2007) Mismatch negativity and stimulus-specific adaptation in animal models. J Psychophysiol 21:214–223.

Paxinos G, Watson C (2005) The rat brain in stereotaxic coordinates. Burlington: Elsevier-Academic.

Pérez-González D, Malmierca MS, Covey E (2005) Novelty detector neurons in the mammalian auditory midbrain. Eur J Neurosci 22:2879–2885. CrossRef Medline

Pérez-González D, Malmierca MS, Moore JM, Hernández O, Covey E (2006) Duration selective neurons in the inferior colliculus of the rat: topographic distribution and relation of duration sensitivity to other response properties. J Neurophysiol 95:823–836. Medline

Pérez-González D, Hernández O, Covey E, Malmierca MS (2012) GABA(A)-mediated inhibition modulates stimulus-specific adaptation in the inferior colliculus. PLoS One 7:e34297. CrossRef Medline

Rees A, Sarbaz A, Malmierca MS, Le Beau FE (1997) Regularity of firing of neurons in the inferior colliculus. J Neurophysiol 77:2945–2965. Medline

Sivaramakrishnan S, Sterbing-D'Angelo SJ, Filipovic B, D'Angelo WR, Oliver DL, Kuwada S (2004) GABA(A) synapses shape neuronal responses to sound intensity in the inferior colliculus. J Neurosci 24:5031–5043. CrossRef Medline

Slabu L, Grimm S, Escera C (2012) Novelty detection in the human auditory brainstem. J Neurosci 32:1447–1452. CrossRef Medline

Slabu L, Escera C, Grimm S, Costa-Faidella J (2010) Early change detection in humans as revealed by auditory brainstem and middle-latency evoked potentials. Eur J Neurosci 32:859–865. CrossRef Medline

Taaseh N, Yaron A, Nelken I (2011) Stimulus-specific adaptation and deviance detection in the rat auditory cortex. PLoS One 6:e23369. CrossRef Medline

Ulanovsky N, Las L, Nelken I (2003) Processing of low-probability sounds by cortical neurons. Nat Neurosci 6:391–398. CrossRef Medline

Ulanovsky N, Las L, Farkas D, Nelken I (2004) Multiple time scales of adaptation in auditory cortex neurons. J Neurosci 24:10440–10453. CrossRef Medline

von der Behrens W, Bäuerle P, Kössl M, Gaese BH (2009) Correlating stimulus-specific adaptation of cortical neurons and local field potentials in the awake rat. J Neurosci 29:13837–13849. CrossRef Medline

Williams AJ, Fuzessery ZM (2011) Differential roles of GABAergic and glycinergic input on FM selectivity in the inferior colliculus of the pallid bat. J Neurophysiol 106:2523–2535. CrossRef Medline

Wu GK, Arbuckle R, Liu BH, Tao HW, Zhang LI (2008) Lateral sharpening of cortical frequency tuning by approximately balanced inhibition. Neuron 58:132–143. CrossRef Medline

Yu XJ, Xu XX, He S, He J (2009) Change detection by thalamic reticular neurons. Nat Neurosci 12:1165–1170. CrossRef Medline

Zhao L, Liu Y, Shen L, Feng L, Hong B (2011) Stimulus-specific adaptation and its dynamics in the inferior colliculus of rat. Neuroscience 181:163–174. CrossRef Medline